Exploiting Photometric Information for Planning under Uncertainty

Gabriele Costante, Jeffrey Delmerico, Manuel Werlberger, Paolo Valigi, and Davide Scaramuzza

Abstract Vision-based localization systems rely on highly-textured areas for achieving an accurate pose estimation. However, most previous path planning strategies propose to select trajectories with minimum pose uncertainty by leveraging only the geometric structure of the scene, neglecting the photometric information (*i.e*, texture). Our planner exploits the scene's visual appearance (*i.e*, the *photometric information*) in combination with its 3D geometry. Furthermore, we assume that we have no prior knowledge about the environment given, meaning that there is no pre-computed map or 3D geometry available. We introduce a novel approach to update the optimal plan *on-the-fly*, as new visual information is gathered. We demonstrate our approach with real and simulated Micro Aerial Vehicles (MAVs) that perform perception-aware path planning in real-time during exploration. We show significantly reduced pose uncertainty over trajectories planned without considering the perception of the robot.

Supplementary Material

A video showing the results of our monocular depth estimation approach is available at `https://www.youtube.com/watch?v=5UmEw8LDJCI`.

Gabriele Costante
University of Perugia, Perugia, Italy, e-mail: `gabriele.costante@studenti.unipg.it`

Jeffrey Delmerico
University of Zürich, Zürich, Switzerland, e-mail: `jeffdelmerico@ifi.uzh.ch`

Manuel Werlberger
University of Zürich, Zürich, Switzerland, e-mail: `werlberger@ifi.uzh.ch`

Paolo Valigi
University of Perugia, Perugia, Italy, e-mail: `paolo.valigi@.unipg.it`

Davide Scaramuzza
University of Zürich, Zürich, Switzerland, e-mail: `sdavide@ifi.uzh.ch`

1 Introduction

We consider the problem of planning an optimal trajectory between two spatial locations in an initially unknown environment with an autonomous, vision-controlled, micro aerial vehicle (MAV). In many previous works, optimal trajectories are those with the shortest or lowest effort path to the goal position. To improve the performance of vision-based control, and consequently all of the other perception functions that rely on the robot's pose estimate, we instead consider optimal trajectories to be those that minimize the uncertainty in this pose estimate. Because we compute the robot pose uncertainty as a function of the photometric information of the scene, we call this approach *Perception-aware Path Planning*.

Despite the impressive results achieved in visual SLAM applications [1, 2], most of vision-controlled MAVs navigate towards a goal location using a predefined set of viewpoints or by remote control, without responding to environmental conditions [3, 4]. Recently, several works have tackled the problem of autonomously planning an optimal trajectory towards a goal location [5, 6], and others have extended this to uncertainty-aware planning that tries to provide high localization accuracy [7, 8]. However, these approaches discard the photometric information (*i.e*, texture) of the scene and plan the trajectory in advance, which requires prior knowledge of the full 3D map of the environment. We propose a system that instead selects *where to look*, in order to capture the maximum visual formation from the scene to ensure pose estimates with low uncertainty.

Additionally, we consider the scenario where the robot has no prior knowledge of the environment, and it explores to generate a map and navigate to a goal. Without an a priori map, we update the planned path as new images are collected by the camera while the robot explores the surroundings (see Figure 1). In particular, we utilize the photometric information in the newly observed regions of the environment to determine the optimal path with respect to pose uncertainty. To the best of our knowledge, this is among the first works that propose to plan a *perception-aware* trajectory *on-the-fly*, while perceiving the environment with only a camera sensor.

We evaluate the proposed methods with several different experiments designed to illustrate the feasibility of our approach for an autonomous MAV, and to demonstrate the improvement in pose uncertainty when planning with perception awareness.

1.1 Related Work

When the minimization of the localization uncertainty is considered in the planning process, the problem is often referred to as "Planning under Uncertainty" or "Planning in Information Space". Probabilistic planning with the inability to directly observe all the state information is often based on Partially Observable Markov Decision Processes (POMDPs) or solved as a graph-search problem. The major drawback of these approaches is their exponential growth in computational complexity. Sim and Roy [9] selected trajectories that maximize the map reconstruc-

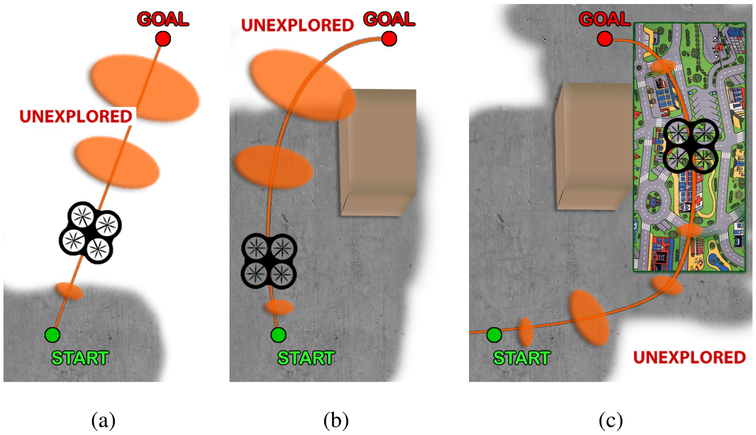

Fig. 1: Online perception-aware path planning: An initial plan is computed without prior knowledge about the environment (a). The plan is then updated as new obstacles (b) or new textured areas (c) are discovered. Although the new trajectory is longer than the one in (b), it contains more photometric information and, thus, is optimal with respect to the visual localization uncertainty.

tion accuracy in SLAM applications. They proposed to use a breadth-first search over possible robot positions to predict a sequence of EKF estimates and select the one that lead to the maximum information gain. Recently, sampling-based methods have been introduced to plan trajectories in complex configuration spaces. Optimal Rapidly-exploring Random Trees (RRT*s) [10] have been widely used in path planning problems and their extension to Rapidly-exploring Random Belief Trees (RRBTs) [7] takes pose uncertainty into account and avoids collisions.

Selecting sequences of viewpoints that optimize for a certain task (*e.g*, pose estimation or map uncertainty minimization) is referred to as *active perception* [11, 12]. While previous papers on active perception relied on using range sensors (*e.g*, [8]), Davison and Murray [13] were among the first to use vision sensors (a stereo camera setup) to select where the camera *should look* to reduce the pose drift during visual SLAM. More recently, Sadat et al. [14] and Achtelik et al. [15] investigated optimal path planning by leveraging visual cues. The former ensures good localization accuracy by extending RRTs* to select feature-rich trajectories, while the latter uses RRBT to compute the propagation of the pose uncertainty by minimizing the reprojection error of 3D map points. Kim and Eustice [16] proposed a Perception Driven Navigation (PDN) framework: the robot follows a pre-planned path and computes information gain at the viewpoints along it, but revisits already-explored, highly-salient areas to regain localization accuracy if its pose uncertainty increases.

It should be noted that all approaches mentioned so far [15, 14, 13, 16] rely on *sparse 2D features* to compute highly-informative trajectories. By contrast, in this paper we rely on *direct methods* [17]. Contrarily to feature-based approaches—which only use small patches around corners—direct methods use all information in the image, including edges. They have been shown to outperform feature-based methods in terms of robustness and accuracy in sparsely-texture scenes [18, 1, 2].

Several works have addressed the problem of online planning. Efficient replanning was addressed in Ferguson et al. [19] by updating the trajectory whenever a new obstacle is spotted. For RRT*, Boardman et al. [20] proposed to dynamically update an initial planned trajectory by computing a new RRT* tree rooted by the robot's current location and reusing branches from the initially-grown tree. Otte and Frazzoli [21] further address the problem of online planning in dynamic environments by modifying the original search graph whenever changes in the environment are observed. Among MAVs, Grzonka et al. [5] considered a quadrotor equipped with an on-board laser scanner, and scanned the environment, adapting the trajectory as new objects were spotted. Similarly, Nieuwenhuisen et al. [6] also used a 3D laser scanner on an autonomous quadrotor to build and update an obstacle map and replan collision-free trajectories. Similar approaches based on different sensors, such as cameras or depth sensors, were proposed in [22]. However, the previous approaches [5, 6, 22] rely on configurations that include other sensors (*e.g*, IMU, Laser Scanner) in addition to cameras. Furthermore, planning is performed without considering the visual perception and, in particular, the photometric information.

1.2 Contribution

In contrast to the previous works, in this paper we propose a novel method to update the optimal trajectory that leverages the *photometric information* (*i.e*, texture) and the 3D structure of newly-explored areas on the fly (*i.e*, *online*), avoiding full replanning. In order to use that information for minimizing pose uncertainty, we perform path planning in four degrees of freedom *(x, y, z, and yaw)*. Furthermore we proposed a novel *textured* volumetric map representation that allows us to efficiently synthesize views to compute the photometric information in the scene and plan accordingly. To the best of our knowledge, this is among the first works to propose a fully autonomous robotic system that performs onboard localization and online perception-aware planning. The main contributions of this paper are:

1. We propose to leverage the *photometric* appearance of the scene, in addition to the 3D structure, to select trajectories with minimum pose uncertainty. The photometric information is evaluated by using *direct* methods. As direct methods use all the information in the image, they provide a more robust and effective way to exploit visual information compared to feature-based strategies.
2. Perception-aware planning is performed online as the robot explores the surroundings, without prior knowledge of the full map of the environment.
3. A novel *textured* volumetric map formulation is proposed to efficiently synthesize views for perception-aware planning.
4. We demonstrate the effectiveness of our approach with experiments in both real-world and simulated environment with a MAV only equipped with vision sensors.

2 Perception-aware Pose Uncertainty Propagation

The visual localization system relies on the availability of texture in the scene to reduce the pose estimation uncertainty. As a consequence, selecting the trajectory that is optimal with respect to the localization accuracy requires evaluation of the pose-uncertainty propagation along a candidate path and the uncertainty reduction associated with the photometric information in the scene.

2.1 Pose Propagation

We represent the pose of the robot as a 6 Degree of Freedom (DoF) transformation matrix $\mathbf{T}$, member of the *special Euclidean group* in $\mathbb{R}^3$, which is defined as follows:

$$\mathrm{SE}(3) := \left\{ \mathbf{T} = \begin{bmatrix} \mathbf{C} & \mathbf{r} \\ \mathbf{0}^T & 1 \end{bmatrix} \middle| \, \mathbf{C} \in \mathrm{SO}(3), \mathbf{r} \in \mathbb{R}^3 \right\}, \tag{1}$$

where $\mathrm{SO}(3)$ is the special orthogonal group in $\mathbb{R}^3$ (the set of spatial rotations, *i.e*, $\mathbf{C}\mathbf{C}^T = \mathbf{1}, \det \mathbf{C} = 1$) and $\mathbf{1}$ is the 3×3 identity matrix. The *Lie Algebra* associated to the $\mathrm{SE}(3)$ Lie Group is indicated as $\mathfrak{se}(3)$. To represent the uncertainty of the robot pose, we define a random variable for $\mathrm{SE}(3)$ members according to:

$$\mathbf{T} := \exp(\boldsymbol{\xi}^{\wedge})\bar{\mathbf{T}}, \tag{2}$$

where $\bar{\mathbf{T}}$ is a noise-free value that represents the pose and $\boldsymbol{\xi} \in \mathbb{R}^6$ is a small perturbation that we assume to be normally distributed $\mathcal{N}(\boldsymbol{\xi}|\mathbf{0}, \boldsymbol{\Sigma})$. We make use of the $\wedge$ operator to map $\boldsymbol{\xi}$ to a member of the Lie algebra $\mathfrak{se}(3)$ (see [23]).

We refer to $\mathbf{T}_{k,w}$ as the robot pose at time k relative to the world frame w and to $\mathbf{T}_{k+1,k}$ as the transformation between the pose at time k and $k+1$.

Assuming no correlation between the current pose and the transformation between k and $k+1$, we can represent $\mathbf{T}_{k,w}$ and $\mathbf{T}_{k+1,k}$ with their means and covariances $\{\bar{\mathbf{T}}_{k,w}, \boldsymbol{\Sigma}_{k,w}\}$ and $\{\bar{\mathbf{T}}_{k+1,k}, \boldsymbol{\Sigma}_{k+1,k}\}$, respectively. Combining them, we get

$$\mathbf{T}_{k+1,w} = \mathbf{T}_{k,w}\ \mathbf{T}_{k+1,k}. \tag{3}$$

To compute the mean and the covariance of the compound pose, we use the results from [23]. The mean and the covariance, approximated to fourth order, are:

$$\bar{\mathbf{T}}_{k+1,w} = \bar{\mathbf{T}}_{k,w}\ \bar{\mathbf{T}}_{k+1,k},\ \boldsymbol{\Sigma}_{k+1,w} \simeq \boldsymbol{\Sigma}_{k,w} + \mathcal{T}\boldsymbol{\Sigma}_{k+1,k}\mathcal{T}^{\top} + \mathcal{F} \tag{4}$$

where $\mathcal{T}$ is $Ad(\bar{\mathbf{T}}_{k,w})$, the adjoint operator for $\mathrm{SE}(3)$, and $\mathcal{F}$ encodes the fourth-order terms. Using Eqn. (4), we propagate the uncertainty along a given trajectory.

2.2 Measurement Update

In contrast to previously published approaches, which mostly rely on *sparse* image features, we use direct methods, in the form of *dense image-to-model alignment*, for

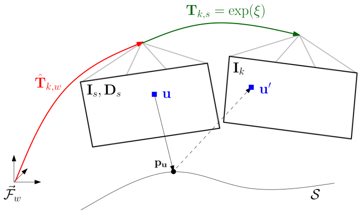

Fig. 2: Illustration of the dense image-to-model alignment used in the measurement update. Given an estimate of the pose $\hat{\mathbf{T}}_{k,w}$, we can synthesize an image and depthmap $\{\mathbf{I}_k, \mathbf{D}_k\}$ from the 3D model $\mathcal{S}$.

the measurement update. Integrating the intensity and depth of *every* pixel in the image enables us to consider photometric information when planning the trajectory.

2.2.1 Preliminary Notation

At each time step of the robot navigation, we can compute a dense surface model $\mathcal{S} \in \mathbb{R}^3 \times \mathbb{R}^+$ (3D position and grayscale intensity) of the explored part of the scene. The rendered synthetic image is denoted with $\mathbf{I}_s : \Omega_s \subset \mathbb{R}^2 \to \mathbb{R}^+$, where Ω_s is the image domain and $\mathbf{u} = (u, v)^T \in \Omega_s$ are pixel coordinates. Furthermore, we refer to the depthmap $\mathbf{D}_s$, associated to an image $\mathbf{I}_s$, as the matrix containing the distance at every pixel to the surface of the scene: $\mathbf{D}_s : \Omega_s \to \mathbb{R}^+; \mathbf{u} \mapsto d_\mathbf{u}$ where $d_\mathbf{u}$ is the depth associated to $\mathbf{u}$. A 3D point $\mathbf{p} = (x, y, z)^T$ in the camera reference frame is mapped to the corresponding pixel in the image $\mathbf{u}$ through the camera projection model $\pi : \mathbb{R}^3 \to \mathbb{R}^2$, $\mathbf{u} = \pi(\mathbf{p})$. On the other hand, we can recover the 3D point associated to the pixel $\mathbf{u}$ using the inverse projection function π^{-1} and the depth $d_\mathbf{u}$:

$$\mathbf{p}_\mathbf{u} = \pi^{-1}(\mathbf{u}, d_\mathbf{u}). \tag{5}$$

Note that the projection function π is determined by the intrinsic camera parameters that are known from calibration. Finally, a rigid body transformation $\mathbf{T} \in \mathrm{SE}(3)$ rotates and translates a point $\mathbf{q}$ to:

$$\mathbf{q}'(\mathbf{T}) := (\mathbf{1} \,|\, \mathbf{0})\, \mathbf{T}\, (\mathbf{q}^T, 1)^T. \tag{6}$$

2.2.2 Dense Image-to-Model Alignment

To refine the current pose estimate, we use *dense image-to-model alignment* [24, 18] (see Fig. 2). This approach computes the pose $\mathbf{T}_{k,w}$ of the synthetic image $\mathbf{I}_s$ by minimizing the photometric error between the observed image and the synthetic one. Once converged, it also provides the uncertainty of the alignment by evaluating the *Fisher Information Matrix*, which we use to select informative trajectories.

The photometric error $r_\mathbf{u}$ for a pixel $\mathbf{u}$ is the difference of the intensity value at pixel $\mathbf{u}$ in the real image acquired at time step k and the intensity value in the synthetic image rendered at the estimated position $\hat{\mathbf{T}}_{k,w}$:

$$r_\mathbf{u} = \mathbf{I}_k(\mathbf{u}) - \mathbf{I}_s(\pi(\mathbf{p}'_\mathbf{u}(\hat{\mathbf{T}}_{k,w}))) \tag{7}$$

The error is assumed to be normally distributed $r_{\mathbf{u}} \sim \mathcal{N}(0, \sigma_i^2)$, where σ_i is the standard deviation of the image noise.

Due to the nonlinearity of the problem, we assume that we have an initial guess of the pose $\hat{\mathbf{T}}_{k,w}$ and iteratively compute update steps $\hat{\mathbf{T}}_{k,w} \leftarrow \exp(\boldsymbol{\xi}^{\wedge})\hat{\mathbf{T}}_{k,w}$, $\boldsymbol{\xi}^{\wedge} \in \mathfrak{se}(3)$ that minimize the error. The update step minimizes the least-squares problem:

$$\boldsymbol{\xi} = \arg\min_{\boldsymbol{\xi}} \sum_{\mathbf{u} \in \Omega_s} \frac{1}{2\sigma_i^2} \Big[\mathbf{I}_k(\mathbf{u}') - \mathbf{I}_s(\pi(\mathbf{p}'_{\mathbf{u}}(\hat{\mathbf{T}}_{k,w}))) \Big]^2, \tag{8}$$

with $\mathbf{p}_{\mathbf{u}}$ given by (5), $\mathbf{p}'_{\mathbf{u}}$ as in (6), and $\mathbf{u}' = \pi\big(\mathbf{p}'_{\mathbf{u}}(\exp(\boldsymbol{\xi}^{\wedge}))\big)$.

Addressing the least-squares problem (8) we can compute the optimal $\boldsymbol{\xi}$ using the Gauss-Newton method and solving the normal equations $\mathbf{J}^T\mathbf{J}\boldsymbol{\xi} = -\mathbf{J}^T\mathbf{r}$, where $\mathbf{J}$ and $\mathbf{r}$ are the stacked Jacobian and image residuals of all pixels $\mathbf{u} \in \Omega_s$, respectively.

At the convergence of the optimization, the quantity

$$\boldsymbol{\Lambda}_k = \frac{1}{\sigma_i^2}\mathbf{J}^T\mathbf{J} \tag{9}$$

is the *Fisher Information Matrix* and its inverse is the covariance matrix $\boldsymbol{\Sigma}_{\mathbf{I}_k}$ of the measurement update. According to [23], we find the covariance matrix after the measurement update at time k by computing

$$\boldsymbol{\Sigma}_{k,w} \leftarrow \Big(\boldsymbol{\Lambda}_k^{-1} + \mathcal{J}^{-T}\boldsymbol{\Sigma}_{k,w}\mathcal{J}^{-1}\Big)^{-1}, \tag{10}$$

where the “left-Jacobian $\mathcal{J}$ is a function of how much the measurement update modified the estimate. Given the information matrix in (9), we define the photometric information gain as $\mathrm{tr}(\boldsymbol{\Lambda}_k)$.

3 Online Perception-aware Path Planning

The framework described in Section 2 is able to predict the propagation of the pose uncertainty along a given trajectory by integrating the photometric information when available. However, to select the *best* sequence of camera viewpoints we need to evaluate all the possible trajectories. As we do not assume to have any given prior knowledge about the scene, the photometric information of the environment, as well as its 3D geometry, are unknown. Hence, the plan that is considered optimal in the beginning, will be adapted as new information is gathered by the robot.

In this section, we describe how we enhance the RRT* [10] with the perception-aware nature that takes benefit from the photometric information to select the trajectory that is optimal with respect to the localization accuracy.

The RRT* incrementally grows a tree in the state space by randomly sampling and connecting points through collision-free edges. Optimality is guaranteed through the *rewire* procedure, which checks for better connections when adding a new point to the tree. The tree is composed of a set of vertices V that represent points in the state space. Each vertex $v = \{x_v, \boldsymbol{\Sigma}_v, \boldsymbol{\Lambda}_v, c_v, p_v\} \in V$ is described via its state $x_v = \mathbf{T}_{v,w}$ (*i.e*, the pose relative to the vertex v with respect to the reference frame w), c_v being the accumulated cost of the trajectory up to v and a unique parent vertex p_v. In addition, we add the pose covariance $\boldsymbol{\Sigma}_v$ and the photometric information $\boldsymbol{\Lambda}_v$ (relative to the camera view associated to the pose x_v) to the vertex v in order to update the pose covariance according to the photometric information.

To select the best path among all possible trajectories $\mathcal{T}_i \in \mathcal{P}$, we minimize:

$$J(\mathcal{T}_i) = \sum_{j=1}^{N_i} \alpha \, \mathrm{Dist}(x_{v^i_j}, x_{v^i_{j-1}}) + (1-\alpha) \, \mathrm{tr}(x_{v^i_j}.\Sigma) \ , \tag{11}$$

where the trajectory is represented by a sequence of N_i waypoints v^i_j, $\mathrm{Dist}(\cdot, \cdot)$ computes the distance between two vertices and α defines the trade-off between this distance and the photometric information gain. Note that we jointly optimize for position and yaw orientation w.r.t. information gain, so the optimal poses are not just the RRT* poses with optimized orientation. We choose the trace to include the visual information into the cost function following the considerations in [25]. In particular, the minimization of the trace of the pose covariance matrix (A-optimality) guarantees that the majority of the state space dimensions are be considered (in contrast to the D-optimality), but does not require us to compute all the eigenvalues (E-optimality). The fundamental steps of the perception-aware RRT* are summarized in Algorithm 1. At each iteration, it samples a new state from the state space and connects it to the nearest vertex (lines 3-19). Next, the function `Near()` checks on the vertices within a ball, centered at the sampled state (see [10]), and propagate the pose covariance from these vertices to the newly sampled one. The one that minimizes the cost function (11) gets selected. Finally, we update the tree connections through the *rewire* procedure. Note that although the optimization is performed on the trace, the full covariance is propagated along each trajectory for evaluation.

Given an initially optimal path, we can now start exploring the environment. When new parts of the scene are revealed, the current trajectory might become non-optimal or even infeasible in case of obstacles. One possibility would be to recompute the tree from scratch after every map update but this would be costly and computationally intractable to have the system integrated into an MAV application. For this reason, we propose to update the planning tree *on-the-fly* by only processing vertices and edges affected by new information. This online update is illustrated in Figure 3 and its fundamental steps are depicted in Algorithm 2. Consider an initial planning tree as in Figure 3(a), that is grown from a starting point (indicated by a green circle) to a desired end point location (the red circle). Whenever a new obstacle is spotted, the respective edge and the affected subtree get invalidated and regrown (lines 04-06) as in Figure 3(b). Note that the `SampleUnexplored()` function is now bounded within the subspace corresponding to the invalidated subtree, which results in a drastically reduced number of iterations compared to fully regrowing the RRT* tree from scratch. The second scenario in Figures 3(d) to 3(f) demonstrates the case of gaining areas with distinctive photometric information. As newly discovered areas provide photometric information, as shown in Figure 3(e), the neighboring vertices are updated by the `RewireTree()` procedure (lines 07-10 in Algorithm 2). Potentially better connections are considered to form a new path with lower costs (Figure 3(f)).

Algorithm 1 Perception-aware RRT*

```
Init: $x_{v_0} = x_{\text{init}}$; $p_{v_0} = \text{root}$; $\boldsymbol{\Sigma}_{v_0} = \boldsymbol{\Sigma}_0$; $c_{v_0}$; $V = \{v_0\}$; Number of iterations $T$
for $t = 1, \ldots, T$ do
  $x_{\text{new}} = \text{SampleUnexplored}()$
  $v_{\text{nst}} = \text{Nearest}(x_{\text{new}})$
  if ObstacleFree$(v_{\text{new}}, v_{\text{nst}})$
    $\Sigma_{\text{t}} = \text{PropagateAndUpdate}(x_{v_{\text{nst}}}, \boldsymbol{\Sigma}_{v_{\text{nst}}}, x_{v_{\text{new}}}, \boldsymbol{\Lambda}_{v_{\text{new}}})$
    $J_{\text{min}} = c_{v_{\text{nst}}} + (1-\alpha)\,\text{tr}(\Sigma_{\text{t}}) + \alpha\text{Dist}(x_{v_{\text{nst}}}, x_{v_{\text{new}}})$
    $v_{\text{min}} = v_{\text{nst}}$
    $V = V \cup v(x_{\text{new}})$
    $V_{\text{neighbors}} = \text{Near}(V, v_{\text{new}})$
    for all $v_{\text{near}} \in V_{\text{neighbors}}$ do
      if CollisionFree$(v_{\text{near}}, v_{\text{new}})$
        $\Sigma_{\text{t}} = \text{PropagateAndUpdate}(x_{v_{\text{near}}}, \boldsymbol{\Sigma}_{v_{\text{near}}}, x_{v_{\text{new}}}, \boldsymbol{\Lambda}_{v_{\text{new}}})$
        if $c_{v_{\text{near}}} + (1-\alpha)\,\text{tr}(\Sigma_{\text{t}}) + \alpha\text{Dist}(x_{v_{\text{near}}}, x_{v_{\text{new}}}) < J_{\text{min}}$
          $J_{\text{min}} = c_{v_{\text{near}}} + (1-\alpha)\,\text{tr}(\Sigma_{\text{t}}) + \alpha\text{Dist}(x_{v_{\text{near}}}, x_{v_{\text{new}}})$
          $\boldsymbol{\Sigma}_{v_{\text{new}}} = \Sigma_{\text{t}}$, $c_{v_{\text{new}}} = J_{\text{min}}$, $v_{\text{min}} = v_{\text{near}}$
        end if
      end if
      ConnectVertices$(v_{\text{min}}, v_{\text{new}})$
    end for
    RewireTree()
  end if
end for
```

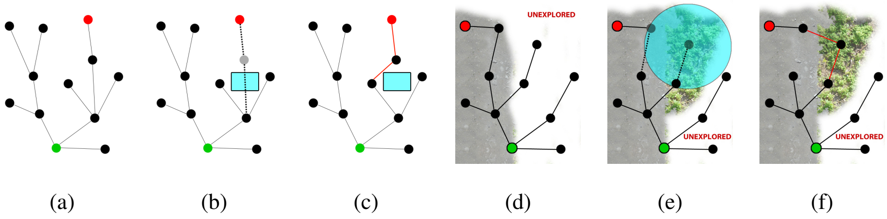

(a) (b) (c) (d) (e) (f)

Fig. 3: Online update steps during exploration: Figures (a)-(c) depict the subtree invalidation and rewiring update when an obstacle is spotted, while (d)-(f) show how the tree is rewired when new photometric information is available from the scene.

Algorithm 2 Online perception-aware RRT*

```
while 1 do
  UpdateCollisionMap()
  UpdatePhotometricInformationMap()
  $V_{\text{colliding}} = \text{NewCollidingVertices}()$
  InvalidateSubTree$(V_{\text{colliding}})$
  Run PerceptionAwareRRT* 1
  $V_{\text{inf}} = \text{UpdatedVertices}()$
  for all $v_{\text{inf}} \in V_{\text{inf}}$ do
    $\boldsymbol{\Lambda}_v = \boldsymbol{\Lambda}_v^{new}$
    RewireTree()
  end for
end while
```

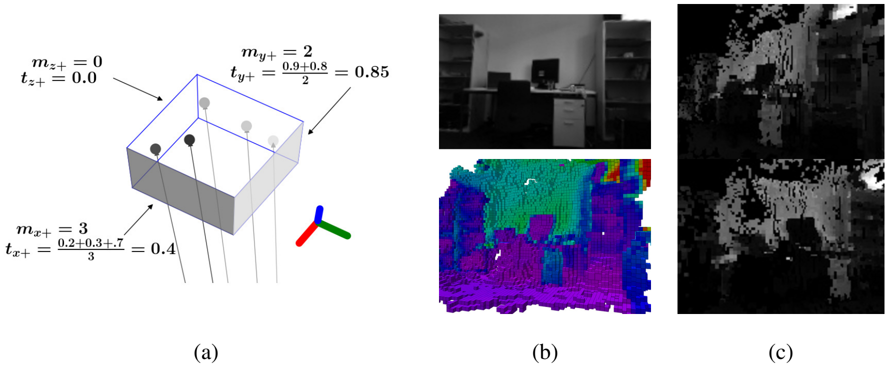
$m_{z+} = 0$
$t_{z+} = 0.0$
$m_{y+} = 2$
$t_{y+} = \frac{0.9+0.8}{2} = 0.85$
$m_{x+} = 3$
$t_{x+} = \frac{0.2+0.3+.7}{3} = 0.4$

(a) (b) (c)

Fig. 4: Textured volumetric mapping: texture information is stored for each face of each voxel in the OctoMap. Each face maintains a mean intensity value for all of the sensor observations that have intersected with it when adding data to the map. (a). A visualization of a *Textured Octomap* is shown in (b), where an office scene was observed with a handheld stereo camera. In (c), we have synthesized some images from the map, at poses that the camera has not yet observed.

4 Textured Volumetric Mapping

We implement an extension to the popular *OctoMap* [26] 3D mapping framework that records texture information within the volumetric map, allowing novel views to be synthesized for perception-aware path planning (see Fig. 4).

We utilize this stored texture to synthesize views of the known map from hypothetical positions for the camera. For each synthetic view, we synthesize an image of what it would look like to observe the environment from that pose—at least up to the currently observed state of the map—and use these synthetic images in the computation of information gain during planning. As an extension to an OctoMap that stores an estimate of occupancy probability for each voxel, we maintain an estimate of the texture for *each face* of each voxel as an intensity value, averaged over all of the observations of that face. We chose this approach because of its compactness—we must only store the current estimate and the number of cumulative observations—and because it is not depth dependent for either updating or querying. It is also directly extensible to a hierarchical representation, such that texture values at higher levels of the octree can be computed from the faces of their child voxels. While our approach to rendering images from a volumetric map is similar to the one in [27], we chose to store texture for the faces, and not just for the volume, because the space represented by a voxel does not necessarily have the same appearance when observed from different sides. Storing more descriptive representations of texture (e.g. Harris corner scores) for the faces would be beneficial, but these metrics are often dependent on the range at which they are observed, presenting a barrier for maintaining a general estimate. The average intensity representation is efficient to update with new observations, efficient to query for the current estimate, and adds only minimal overhead to the computation required for mapping.

Our update method proceeds as follows. Given an input point cloud, occupancy is updated as in [26], where ray casting from the sensor origin is used to update each leaf voxel along the ray, until the observed point, and each leaf voxel is updated at most once for occupancy. To update the texture, for each point p_i^k in the k^{th} point cloud C^k, we determine the face f that its ray intersects in the leaf voxel n containing p_i^k. At leaf voxel n, we maintain the current intensity estimate t_f and number of cumulative observations m_f for each face $f \in 1 \ldots 6$ of the voxel cube (see Fig. 4(a)). After the insertion of k point clouds, these quantities are:

$$m_f^k = \sum_{j=1}^{k} \left| p_i^j \in n \right|, \qquad t_f^k = \frac{\sum_{j=1}^{k} t_{p_i^j} \in f}{m_f} \tag{12}$$

This can be updated efficiently for each new point cloud input:

$$m_f^{k+1} = m_f^k + \left| p_i^{k+1} \in n \right|, \qquad t_f^{k+1} = \frac{m_f^k t_f^k + t_{p_i^k}}{m_f^{k+1}} \tag{13}$$

The inclusion of texture in the OctoMap requires an additional computational overhead of only 15% for both insertion and querying.

Storing texture in a volumetric map allows us to hypothesize about the photometric information that our robot could obtain if it moved to a particular pose. We do this by synthesizing images of the map from a hypothetical pose, casting rays through each pixel in the image into the map (See Fig. 4(c)). When these rays intersect with the face of an occupied voxel, we record the texture of the face and the depth to that voxel in intenisty and depth images. These synthetic images are generated for each sampled pose when the planner generates or rewires the tree.

5 System Overview

We consider an MAV that explores an unknown environment by relying only on its camera to perform localization, dense scene reconstruction and optimal trajectory planning. We have integrated the online perception-aware planner with two different mapping systems (see Figure 5): a monocular dense reconstruction system that generates a point cloud map, and a volumetric system that uses stereo camera input.

In the monocular system, the localization of the quadrotor runs onboard, providing the egomotion estimation to perform navigation and stabilization. To achieve real-time performance, the dense map reconstruction and the online perception-aware path planning runs off-board on an Intel i7 laptop with a GPU, in real-time.

At each time step k, the quadrotor receives a new image to perform egomotion estimation. We use the Semi-direct monocular Visual Odometry (SVO) proposed in [2], which allows us to estimate the quadrotor motion in real-time. The computed pose $\mathbf{T}_{k,w}$ and the relative image are then fed into the dense map reconstruction module (REMODE [28], a probabilistic, pixelwise depth estimate to compute dense depthmaps). Afterwards, the dense map provided by the reconstruction module is sent to the path planning pipeline and is used to update both the collision map (using Octomap [26]) and the photometric information map. The last one is then used to update $\boldsymbol{\Lambda}_v$ for each vertex affected by the map update. Finally, we update the optimal trajectory following the procedure described in Algorithm 2.

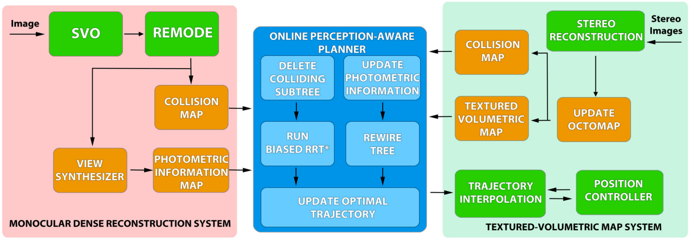

Fig. 5: Block diagram of the online perception-aware planning system.

For the textured volumetric map system, we take input from a stereo camera, perform egomotion estimation with SVO as above, and compute a dense depth map with OpenCV's Block Matcher. The estimated camera pose from SVO and the point cloud produced from the depth map are used to update the Textured OctoMap as in Sec. 4. This volumetric map serves as a collision map, when it is queried for occupancy, and is used to synthesize views and compute photometric information gain during planning, when it is queried for texture. This pipeline runs in real time onboard an MAV's embedded single board computer (an Odroid XU3 Lite) using a map with $5cm$ resolution, and with the input images downsampled by a factor of 4 to 188 × 120, and throttled down to $1Hz$. However, we evaluate this system in simulation, and for the experiments in Sec. 6.2, we run the simulation, visual pipeline, planner, and control software all on a laptop with an Intel i7.

6 Experiments

6.1 Real World Experiments

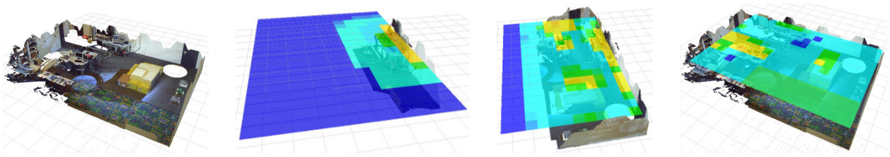

(a) (b) (c) (d)

Fig. 6: Computed photometric information gain at different exploration stages (Figs. (b), (c) and (d)) for the scene in Fig. (a). Warm (yellowish) colors refer to camera viewpoints exhibiting a higher amount of texture, while the cool (bluish) ones indicate less informative areas.

We motivate our approach by discussing how the photometric information distribution changes over time when exploring an unknown environment. Figure 6 shows the map for the photometric information gain at different exploration stages. In Fig. 6(b) the almost unexplored scene has very little valuable information to compute a reliable plan. Standard planners, which calculate trajectories only once without performing online updates, compute sub-optimal plans or even collide with undiscovered objects. Hence, an online approach is needed to re-plan as new photometric information is gathered (see Figs. 6(c) and 6(d)).

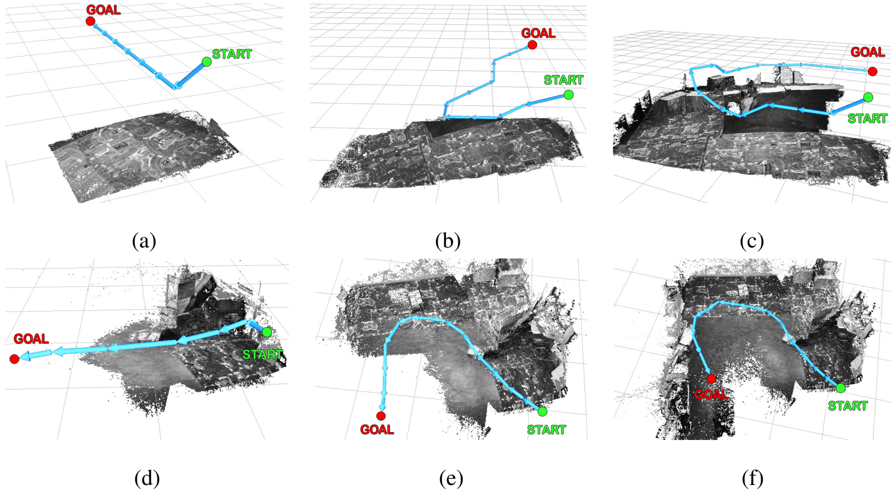

Fig. 7: Experimental results in two real scenarios (rows). The first column shows the initially computed trajectories, only having little information of the environment available. The second and third column demonstrate the update of the plan as new information is gathered by updating the scene.

To evaluate the proposed online perception-aware path planning, we ran experiments on an indoor environment with different configurations. We set up two scenarios with different object arrangements to vary the texture and the 3D structure of the scene. In the first scenario, the monocular camera on the MAV is downward-looking, while in the last one we choose a front-looking monocular configuration with an angle of 45 degrees with respect to the ground plane. We made experiments with two different camera setups to investigate the influence of the camera viewpoint on the optimal trajectory computation. Intuitively, the front-looking configuration provides more information since also areas far from the quadrotor are observed. Conversely, with the downward-looking configuration, the pose estimation algorithm is more reliable, but less information is captured from the scene. Finally, in all the experiments we set $\alpha = 0.1$ to increase the importance of the pose uncertainty minimization.

In all the scenarios, we put highly-textured carpets and boxes along the walls, while the floor in the center of the room is left without texture (*i.e*, with a uniform color). In the first scenario, we also put an obstacle in the center of the room. At the beginning of the exploration, the planner shows similar behavior in all the experiments (see Figs. 7(a) and 7(d)). The information about the scene is very low, thus, our approach computes a simple straight trajectory to the goal. As the robot explores the environment, the plan is updated by preferring areas with high photometric information (cf. Figs. 7(b) and 7(c)). In the second scenario, a front-looking camera provides photometric information about areas distant from the current MAV pose. As a consequence, we obtain an optimal plan earlier with respect to the first experiment (see Figs. 7(e) and 7(f)).

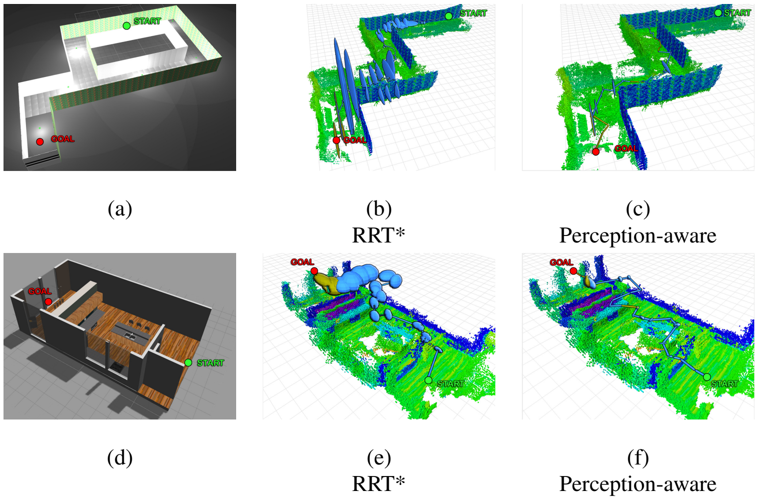

(a)

(b) RRT*

(c) Perception-aware

(d)

(e) RRT*

(f) Perception-aware

Fig. 8: Exploration trial in the *labyrinth* (a) and in the *kitchen* (d) simulated environments. The trajectories computed by the RRT* planner are shown in Fig. (b) for the labyrinth scenario and in Fig. (e) for the kitchen, while the ones computed with the perception aware planner are shown in (c) and in (f), respectively. The Textured OctoMaps are visualized with a color corresponding to the mean intensity over all of the observed faces, with red representing high intensity, and purple representing low intensity. The pose covariance at each waypoint is shown as an ellipse, with the most recent update in orange, and the rest of the plan in blue.

6.2 Simulated Experiments

We demonstrate the proposed system in a simulated environment, using the components described in Sec. 5. Two trials were performed in environments simulated with *Gazebo*, one designed to explicitly test perception (*labyrinth*) and one designed to simulate a real world environment (*kitchen*). The labyrinth scenario is designed with flat and highly-textured walls to test the capability of our perception-aware planner to choose the MAV orientations that maximize the amount of photometric information. The quadrotor starts in one of the two long corridors in the scene (see 8(a)) and is asked to reach the goal location that is located at $25m$ from the start location. In the kitchen world (see 8(d)), the MAV begins at a position that is separated by two walls from the goal location, which is $12.5m$ away. We compare the performance of the standard RRT* planner and our perception-aware planner in Figs. 8 and 9.

6.3 Discussion

The qualitative results shown for the real world (Fig. 7) and simulated (Fig. 8) experiments show that the perception aware planner does indeed choose trajectories that allow the MAV to observe more photometric information. Quantitatively, this results in a dramatic improvement in the uncertainty of the vehicle's pose estimate. The results in Fig. 9 show that the pose uncertainty, measured as the trace of the

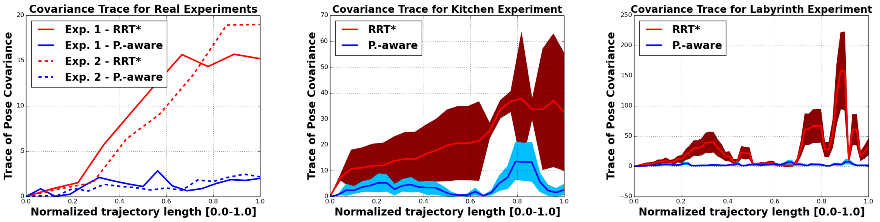

(a) (b) (c)

Fig. 9: Quantitative results for our experiments showing the evolution of the MAV's pose covariance during the planned trajectory. Fig. (a) shows results of the real world experiments. Figs. (b) and (c) show the simulated *kitchen* and *labyrinth* trials, respectively. The plans for each trial result in different length trajectories, so the length of each trajectory is normalized to one. For each simulated experiment, we conducted 15 trials, normalized the trajectories, and inferred Gaussian distributions at each point in a set of equally-spaced samples along a normalized trajectory. In (b) and (c), each solid line represents the mean over all of the trials, and the colored band is the 95% confidence interval.

covariance matrix and vizualized as ellipses in Fig. 8, is up to an order of magnitude smaller when the planner considers the texture of the environment.

In both of the simulated experiments, the RRT* and perception aware planners both reached the goal location in all trials. On average, for the *labyrinth* it took $718.3s$ and $715.2s$, respectively, and for *kitchen* it took $578.3s$ and $580.4s$, respectively. The results are shown in Figs. (8(b)) and 8(c) for the labyrinth tests and in Figs. 8(e) and 8(f) for the kitchen ones. The most important distinction in this performance comparison is the pose uncertainty across the trajectory. The two planners produce similar trajectories in terms of waypoint positions, but the covariances for the RRT* trajectory are much larger due to the desired yaw angles that are chosen for the waypoints. The proposed perception aware planner specifically optimizes the waypoint position and yaw angle (i.e. *where to look*) in order to minimize this pose uncertainty. As a consequence, the plan computed with our strategy has low pose uncertainty values, while the RRT* trajectory, which does not consider the visual information, leads to very low localization accuracy, which can make the navigation infeasible due to the high risk of collisions.

7 Conclusions

We have proposed a novel approach for performing online path planning that leverages the photometric information in the environment to plan a path that minimizes the pose uncertainty of a camera-equipped MAV that is performing vision-based egomotion estimation. These advances include a perception-aware path planner and a textured volumetric map. This planning framework has been evaluated with real and simulated experiments, and both the qualitative and quantitative results support the conclusion that taking photometric information into account when planning significantly reduces a vision-controlled MAV's pose uncertainty. Utilizing perception awareness will enable more robust vision-controlled flight in arbitrary environments.

References

[1] Jakob Engel, Thomas Schöps, and Daniel Cremers. LSD-SLAM: Large-Scale Direct Monocular SLAM. In *European Conference on Computer Vision (ECCV)*, pages 834–849. 2014.

[2] Christian Forster, Matia Pizzoli, and Davide Scaramuzza. SVO: Fast Semi-Direct Monocular Visual Odometry. In *IEEE International Conference on Robotics and Automation (ICRA)*, 2014.

[3] Stephan Weiss, Markus W Achtelik, Simon Lynen, Michael C Achtelik, Laurent Kneip, Margarita Chli, and Roland Siegwart. Monocular Vision for Long-term Micro Aerial Vehicle State Estimation: A Compendium. *Journal of Field Robotics*, 30(5):803–831, 2013.

[4] D. Scaramuzza, M.C. Achtelik, L. Doitsidis, F. Fraundorfer, E. B. Kosmatopoulos, A. Martinelli, M. W. Achtelik, M. Chli, S.A. Chatzichristofis, L. Kneip, D. Gurdan, L. Heng, G.H. Lee, S. Lynen, L. Meier, M. Pollefeys, A. Renzaglia, R. Siegwart, J. C. Stumpf, P. Tanskanen, C. Troiani, and S. Weiss. Vision-Controlled Micro Flying Robots: from System Design to Autonomous Navigation and Mapping in GPS-denied Environments. *IEEE Robotics and Automation Magazine*, 2014.

[5] Slawomir Grzonka, Giorgio Grisetti, and Wolfram Burgard. A Fully Autonomous Indoor Quadrotor. *IEEE Transactions on Robotics*, 28(1):90–100, February 2012.

[6] Matthias Nieuwenhuisen, David Droeschel, Marius Beul, and Sven Behnke. Obstacle Detection and Navigation Planning for Autonomous Micro Aerial Vehicles. In *2014 International Conference on Unmanned Aircraft Systems (ICUAS)*, pages 1040–1047. IEEE, 2014.

[7] Adam Bry and Nicholas Roy. Rapidly-exploring random belief trees for motion planning under uncertainty. In *IEEE International Conference on Robotics and Automation (ICRA)*, pages 723–730, 2011.

[8] Abraham Bachrach, Samuel Prentice, Ruijie He, Peter Henry, Albert S Huang, Michael Krainin, Daniel Maturana, Dieter Fox, and Nicholas Roy. Estimation, planning, and mapping for autonomous flight using an RGB-D camera in GPS-denied environments. *The International Journal of Robotics Research*, 31(11):1320–1343, 2012.

[9] Robert Sim and Nicholas Roy. Global a-optimal robot exploration in slam. In *IEEE International Conference on Robotics and Automation (ICRA)*, pages 661–666, April 2005.

[10] Sertac Karaman and Emilio Frazzoli. Sampling-based algorithms for optimal motion planning. *The International Journal of Robotics Research*, 30(7):846–894, 2011.

[11] Shengyong Chen, Youfu Li, and Ngai Ming Kwok. Active vision in robotic systems: A survey of recent developments. *International Journal of Robotics Research*, 30(11):1343–1377, 2011.

[12] Stefano Soatto. Actionable information in vision. In *Machine Learning for Computer Vision*, pages 17–48. Springer, 2013.

[13] Andrew J Davison and David W Murray. Simultaneous localization and map-building using active vision. *IEEE Transactions on Pattern Analysis and Machine Intelligence*, 24(7):865–880, 2002.

[14] Seyed Abbas Sadat, Kyle Chutskoff, Damir Jungic, Jens Wawerla, and Richard Vaughan. Feature-Rich Path Planning for Robust Navigation of MAVs with Mono-SLAM. In *IEEE International Conference on Robotics and Automation (ICRA)*, 2014.

[15] Markus W Achtelik, Simon Lynen, Stephan Weiss, Margarita Chli, and Roland Siegwart. Motion-and Uncertainty-aware Path Planning for Micro Aerial Vehicles. *Journal of Field Robotics*, 31(4):676–698, 2014.

[16] Ayoung Kim and Ryan M Eustice. Perception-driven navigation: Active visual slam for robotic area coverage. In *IEEE International Conference on Robotics and Automation (ICRA)*, pages 3196–3203. IEEE, 2013.

[17] M. Irani and P. Anandan. All About Direct Methods. In *Vision Algorithms: Theory and Practice*, pages 267–277. Springer, 2000.

[18] Richard A. Newcombe, Steven J Lovegrove, and Andrew J Davison. DTAM: Dense Tracking and Mapping in Real-Time. *IEEE International Conference on Computer Vision (ICCV)*, pages 2320–2327, 2011.

[19] Dave Ferguson, Nidhi Kalra, and Anthony Stentz. Replanning with rrts. In *IEEE International Conference on Robotics and Automation (ICRA)*, pages 1243–1248. IEEE, 2006.

[20] Beth Leigh Boardman, Troy Anthony Harden, and Sonia Martinez. Optimal kinodynamic motion planning in environments with unexpected obstacles. Technical report, Los Alamos National Laboratory (LANL), 2014.

[21] Michael Otte and Emilio Frazzoli. RRT-X: Real-time motion planning/replanning for environments with unpredictable obstacles. In *International Workshop on the Algorithmic Foundations of Robotics (WAFR)*, 2014.

[22] Korbinian Schmid, Philipp Lutz, Teodor Tomić, Elmar Mair, and Heiko Hirschmüller. Autonomous vision-based micro air vehicle for indoor and outdoor navigation. *Journal of Field Robotics*, 31(4):537–570, 2014.

[23] Timothy D Barfoot and Paul T Furgale. Associating Uncertainty with Three-Dimensional Poses for use in Estimation Problems. *IEEE Transactions on Robotics*, 2014.

[24] Maxime Meilland and Andrew I. Comport. On unifying key-frame and voxel-based dense visual SLAM at large scales. In *IEEE International Conference on Intelligent Robots and Systems (IROS)*, 2013.

[25] Sebastian Haner and Anders Heyden. Optimal view path planning for visual slam. In *Image Analysis*, pages 370–380. Springer, 2011.

[26] Armin Hornung, Kai M Wurm, Maren Bennewitz, Cyrill Stachniss, and Wolfram Burgard. Octomap: An efficient probabilistic 3d mapping framework based on octrees. *Autonomous Robots*, 34(3):189–206, 2013.

[27] Julian Mason, Susanna Ricco, and Ronald Parr. Textured Occupancy Grids for Monocular Localization Without Features. In *IEEE International Conference on Robotics and Automation (ICRA)*, Shanghai, China, 2011.

[28] Matia Pizzoli, Christian Forster, and Davide Scaramuzza. REMODE: Probabilistic, Monocular Dense Reconstruction in Real Time. In *IEEE International Conference on Robotics and Automation (ICRA)*, pages 2609–2616. IEEE, May 2014.